Monitoring the Conformational Changes of Photoactivated Rhodopsin from Microseconds to Seconds by Transient Fluorescence Spectroscopy[†]

Daniel Hoersch, Harald Otto, Ingrid Wallat, and Maarten P. Heyn*

Biophysics Group, Department of Physics, Freie Universität Berlin, Arnimallee 14, 14195 Berlin, Germany

Received July 25, 2008; Revised Manuscript Received September 14, 2008

ABSTRACT: The transient changes of the tryptophan fluorescence of bovine rhodopsin in ROS membranes were followed in time from 1 μs to 10 s after flash excitation of the photoreceptor. Up to about 100 μs the fluorescence did not change, suggesting that the tryptophan lifetimes in rhodopsin and the M_I intermediate are similar. The fluorescence then decreases on the millisecond time scale with kinetics that match the rise of the M_{II} state as measured on the same sample by the transient absorption increase at 360 nm. Both the sign and kinetics of the fluorescence change strongly suggest that it is due to an increase in energy transfer to the retinylidene chromophore caused by the increased spectral overlap in M_{II}. Calculation of the Förster radius of each tryptophan from the high-resolution crystal structure suggests that W265 and W126 are already completely quenched in the dark, whereas W161, W175, and W35 are located at distances from the retinal chromophore that are comparable to their Förster radii. The fluorescence from these residues is thus sensitive to an increase in energy transfer in M_{II}. Similar results were obtained at other temperatures and with monomeric rhodopsin in dodecyl maltoside micelles. A large light-induced transient fluorescence increase was observed with ROS membranes that were selectively labeled with Alexa594 at cysteine 316 in helix 8. Using transient absorption spectroscopy the kinetics of this structural change at the cytoplasmic surface was compared to the formation of the signaling state M_{II} (360 nm) and to the kinetics of proton uptake as measured with the pH indicator dye bromocresol purple (605 nm). The fluorescence kinetics lags behind the deprotonation of the Schiff base. The proton uptake is even further delayed. These observations show that in ROS membranes (at pH 6) the sequence of events is Schiff base deprotonation, structural change, and proton uptake. From the temperature dependence of the kinetics we conclude that the Schiff base deprotonation and the transient fluorescence have comparable activation energies, whereas that of proton uptake is much smaller.

Rhodopsin, the photoreceptor of rod cells, is a member of the large family of G-protein-coupled receptors with the structural motif of a transmembrane heptahelical bundle (for a review see ref *1*). The interhelical loops on the cytoplasmic surface are essential for transient recognition and binding of signaling proteins. In the dark the retinylidene chromophore is covalently linked to lysine 296 of opsin via a protonated Schiff base (SB)[1] ($\lambda_{max} \sim 500$ nm) and is in the 11-cis configuration. The crystal structures of the dark state (*2*−*5*) and of several intermediates (*6, 7*) have been solved (see Figure 1). Absorption of light leads to rapid photoisomerization of the 11-*cis*-retinal to the all-trans form (*8*) and is followed by a series of slower structural relaxations involving the intermediates batho-, lumi- and meta I-rhodopsin. M_I is in a pH- and temperature-dependent equilibrium with the signaling state M_{II}. This equilibrium is established in milliseconds (*9, 10*). In the transition from M_I to M_{II} the Schiff base linkage is deprotonated, which is accompanied by a major blue shift of the chromophore absorption maximum to 380 nm. No high-resolution structure is available as yet for the active state M_{II}. Low-resolution structural information has been mainly obtained from ESR spectroscopy with spin labels (*12*). The initial chromophore

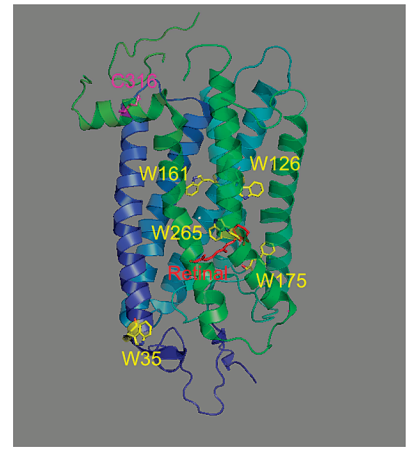

FIGURE 1: Backbone crystal structure of bovine rhodopsin based on Protein Data Bank file 1F88. The five tryptophans (yellow), the retinal (red), and C316 in helix 8 (magenta), the attachment site for the fluorescence label Alexa594, are shown as sticks. The image was prepared using the program Pymol.

[†] This work was supported by DFG Grant He1382/14-2 (to M.P.H. and H.O.).

* Corresponding author: phone, 49-30-83856160; fax, 49-30-83856299; e-mail, heyn@physik.fu-berlin.de.

[1] Abbreviations: DM, dodecyl maltoside; LED, light emitting diode; BCP, bromocresol purple; ROS, rod outer segment; SB, Schiff base; PM, photomultiplier.

10.1021/bi801397e CCC: $40.75
Published on Web 10/11/2008

switching event, localized in the chromophore binding pocket, triggers a sequence of thermal protein relaxations which culminates in M_{II} in a global conformational change involving the cytoplasmic surface domains, helix 8, and a rigid body motion of transmembrane helix VI (*1, 12*). Moreover, during the lifetime of M_{II} proton uptake occurs from the cytoplasmic surface most likely by glutamate 134 in the ERY motif (*13*−*16*). The timing of these three events involving the M_{II} state (SB deprotonation, conformational change, proton uptake) is of great interest. It was found that proton uptake is delayed with respect to SB deprotonation (*13*). It was recently shown, by time-resolved ESR spectroscopy with rhodopsin in DM micelles, that SB deprotonation precedes the rotational motion of helix VI, which occurs with the same kinetics as proton uptake (*9*). For rhodopsin in the native ROS membranes similar data are not available.

The dynamics of the structural changes of rhodopsin has been mainly monitored by time-resolved absorption and ESR spectroscopy (*9*−*11, 14, 17*). Transient absorption spectroscopy has high time resolution and good signal-to-noise ratio but is limited to the absorption changes occurring at the retinylidene chromophore. ESR spectroscopy requires the introduction of spin labels and has the disadvantage of low signal-to-noise ratio, which effectively limits the time resolution to milliseconds (*9, 17*). Time-resolved FTIR difference spectroscopy is technically very challenging for a noncyclic photosystem such as rhodopsin (*18*) and has not found widespread application.

Fluorescence offers an alternative method to monitor conformational and environmental changes. Fluorescence is very sensitive, allowing high time resolution. It allows the reporting of local structural events by using fluorescence labels bound to the reactive SH groups of cysteines (either the native accessible and reactive cysteines 140 and 316 or cysteines introduced by mutagenesis). Rhodopsin contains moreover five native tryptophans at various positions in the structure (see Figure 1).

Transient fluorescence measurements with rhodopsin are rare and so far limited to the time scale of minutes. It is well-known that the tryptophan fluorescence of rhodopsin is strongly quenched by radiationless energy transfer to the retinylidene chromophore (*19, 20*). In the decay of M_{II} the SB linkage hydrolyzes and retinal is released from the binding pocket. This is accompanied by a large increase in fluorescence. This effect is used as an assay to monitor the decay kinetics of M_{II} (*20*−*22*). The characteristic time constant of the fluorescence increase is about 15 min (*20, 21*). When helix 8 was labeled at cysteine 316 with Alexa594, a 20% increase in fluorescence was observed in the light, presumably associated with the formation of the slowest intermediate M_{II} (*23*). This fluorescence increase could not be time-resolved (*23*).

We recently demonstrated the usefulness of transient fluorescence with the photoreceptor photoactive yellow protein (PYP) which contains a single tryptophan (*24*). Here we used transient fluorescence with microsecond time resolution and applied it to two functionally relevant questions for rhodopsin in ROS membranes. First, we used the natural tryptophans to monitor the fluorescence changes at these sites (Figure 1) during the lifetime of M_I and M_{II}. W265 is an example of a tryptophan in the chromophore binding pocket that experiences a change in position and orientation after chromophore isomerization (*25*−*27*). Second, we used the fluorescence of Alexa594 attached at cysteine 316 to monitor the dynamics of the structural changes of helix 8 in ROS membranes. To compare these kinetics with those detected at other sites, we employed the complementary method of transient absorption spectroscopy to monitor the SB deprotonation and to follow the proton uptake using the pH-sensitive dye bromocresol purple (BCP).

MATERIALS AND METHODS

Materials. Bovine retinas were purchased from J. A. Lawson Corp., and AlexaFluor594 C_5-maleimide was from Molecular Probes. Bromocresol purple was from Sigma and dodecyl maltoside (DM) from Anatrace.

Protein Purification. ROS membranes were prepared from bovine retinas and purified by a stepwise sucrose gradient method (*28*). ROS were washed twice by 50 mM sodium phosphate buffer, pH 7.0, and once with 4 M urea to remove peripheral proteins of the visual cascade. For the Trp fluorescence experiments the membranes were then washed twice in buffer A (5 mM Tris-HCl and 0.5 mM $MgCl_2$, pH 7.2) and twice in 10 mM MES buffer, pH 6. For the proton uptake experiments the membranes were first washed in buffer A and then in buffer B (1 mM Tris-HCl and 0.1 mM $MgCl_2$, pH 7.2) and finally twice in water. BCP dissolved in ethanol was then added to the solution to a final concentration of 100 μM (respectively 50 μM for the temperature variation measurements). The rhodopsin micelles were prepared by washing the ROS membranes twice in buffer C (137 mM NaCl, 2.7 mM KCl, 1.5 mM KH_2PO_4, 8 mM Na_2HPO_4, pH 6.0) and solubilized in buffer C containing 1% DM. The solution was then incubated overnight at 4 °C while mixing (*29*).

Site-Specific Labeling of C316 with Alexa594-maleimide. Site-specific labeling of ROS membranes with Alexa594-maleimide was performed as described (*23*). ROS membranes were washed twice with 50 mM sodium phosphate buffer, pH 7.0 (as described above). Alexa594-maleimide dissolved in DMSO was then added to the ROS membranes in a molar label to rhodopsin ratio of 2:1. The mixture (with less than 3% DMSO in the solution) was incubated overnight at room temperature. The reaction was terminated with glutathione and the mixture kept on ice for 30 min to inactivate the maleimide. The modified membranes were then washed once with 4 M urea, twice with buffer A, and twice with 10 mM MES buffer, pH 6.0.

Transient Fluorescence Spectroscopy. These measurements were performed with a modification of our setup for transient absorption spectroscopy (*30*) shown in Figure 2 and described in more detail in ref *24*. For the transient tryptophan fluorescence the fluorophore is excited by an LED emitting at 280 nm with a half-width of 10 nm. The emission is detected by a photomultiplier (PM), and the time course of this signal is recorded from 1 μs to seconds after exciting the sample with a 20 ns flash at 460 or 500 nm from an excimer-dye laser (*24, 30*). In order to protect the PM from stray light from the LED and the excitation flash the filters WG305 and UG11 (both Schott) were placed in front of it. In this way the evolution of the steady-state fluorescence of the tryptophans during the photoactivation is recorded. The cuvette was placed in a thermostated sample holder. For the

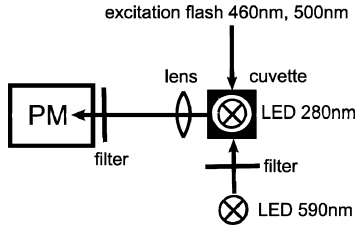

FIGURE 2: Setup for the transient fluorescence measurements. The sample is illuminated either from above with an LED emitting at 280 nm for the Trp fluorescence experiment or from the side with a high-power LED emitting at 590 nm for the Alexa594 fluorescence experiment. In the latter case in addition the filter RG610 is placed between the LED and the cuvette to prevent the activation of rhodopsin by the intense excitation light. In both cases the fluorescence light is collected under an angle of 90° and detected by a photomultiplier tube (PM). The 10 ns excitation pulse at 460 or 500 nm that triggers the photoactivation of rhodopsin enters the cuvette from the side. To protect the PM from stray light from the LEDs and from the scattered excitation light pulses, the filters WG 305 and UG11 (for Trp fluorescence) or GG515 and an interference filter with a transmission maximum at 638 nm and a half-width of 18.5 nm (for Alexa594 fluorescence) were placed in front of the PM.

transient Alexa594 fluorescence measurements this setup was slightly modified. As excitation light source we used a high-power LED emitting at 590 nm with a half-width of 20 nm, which illuminated the sample from the side (see Figure 2). To avoid photoactivation of rhodopsin by the intense LED light, the color filter RG610 (Schott) was placed between the light source and the cuvette. Instead of WG305 and UG11 we placed the color filter GG515 and an interference filter with a transmission maximum at 638 nm and a half-width of 18.5 nm (both Schott) in front of the PM to select the fluorescence and block stray light from the LED and from the excitation pulse.

The transient fluorescence signal $\Delta F/F_0 = (F(t) - F_0)/F_0 = (I(t) - I_0)/I_0$ is defined as the difference of the fluorescence intensity before (F_0) and after ($F(t)$) the laser flash which triggers the photoactivation at $t = 0$, normalized by F_0. It is calculated from the PM current ($I(t)$, I_0).

Fluorescence Resonance Energy Transfer. Radiationless energy transfer is well understood theoretically and well established experimentally. The rate of energy transfer k_T is given by

$$k_T = (8.71 \times 10^{23})\left(\frac{J\kappa^2}{n^4 R_{DA}^{\ 6}}\right)\left(\frac{\Phi_D}{\tau_D}\right) s^{-1} \quad (1)$$

J is the spectral overlap integral between the emission spectrum of the donor and the absorption spectrum of the acceptor, in units of $cm^3\ M^{-1}$. κ^2 is the angular factor of the interaction between the transition dipole moments of the donor ($\vec{\mu}_D$) and acceptor ($\vec{\mu}_A$). Using the angles α, β, and δ defined in Figure 3 we have

$$\kappa^2 = (\cos\beta - 3\cos\alpha\cos\delta)^2 \quad (2)$$

Depending on the values of α, β, and δ, κ^2 varies between 0 and 4. n is the index of refraction. R_{DA} is the distance between the transition dipole moments of donor and acceptor in angstroms (see Figure 3). τ_D is the fluorescence lifetime of the donor in the absence of the acceptor in seconds. Φ_D is the fluorescence quantum yield of the donor in the absence of the acceptor. According to eq 1 the rate constant for energy transfer is proportional to the product of J and κ^2.

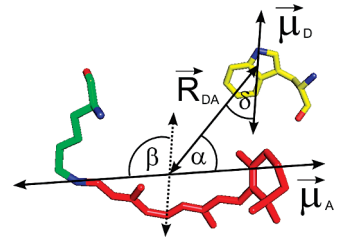

FIGURE 3: Transition dipole moment geometry of the donor−acceptor pair tryptophan 161 and the retinylidene chromophore bound to Lys 296 from 1F88. $\vec{R}_{DA}$ is the vector from donor to acceptor. $\vec{\mu}_A$ was constructed by connecting the nitrogen of the Schiff base and C5 of the retinal as the ends of the conjugated π-electron system of the chromophore (*32*). The orientation of $\vec{\mu}_D$ in the molecular framework of the tryptophan is discussed in detail in ref *31*. The values of α, β, and δ derived from the X-ray diffraction structure for each tryptophan−retinal pair are used to calculate the κ^2 values according to eq 2 and are listed together with R_{DA} and R_0 in Table 1.

Table 1: Trp−Retinal Energy Transfer Parameters Calculated from the Rhodopsin Structure 1U19[a]

Trp	R_{DA}/Å	κ^2	R_0/Å	τ_i/τ_D
35	23.5	1.15	27.4	0.28
126	14.7	1.65	29.1	0.02
161	16.0	0.0007	8.0	0.98
175	18.1	0.37	22.7	0.20
265	4.9	1.32	28.0	0.00003

[a] R_{DA}, distance between donor and acceptor transition dipole moments; κ^2, calculated according to eq 2; R_0, Förster radius; τ_i/τ_D, calculated Trp fluorescence lifetime τ_i normalized by the lifetime τ_D in the absence of energy transfer.

Transient Absorption Spectroscopy. Flash spectroscopy was performed as described elsewhere (*30*). Proton uptake kinetics was monitored at 605 nm using the pH indicator dye bromocresol purple as described (*42*).

RESULTS

Transient Tryptophan Fluorescence in ROS Membranes. A typical time trace of the transient fluorescence from the tryptophans of rhodopsin in ROS membranes at pH 6 (23 °C) is shown in Figure 4A. $\Delta F(t)/F_0$, the ratio of the change in fluorescence and the initial fluorescence before the flash, is plotted against the time. From 1 to about 80 μs, $\Delta F/F_0$ is within experimental error zero, suggesting that the tryptophans do not experience structural or environmental changes in the M_I state. Starting around 80 μs after flash excitation the fluorescence decreases, reaching a plateau value around 20 ms. Note that this stationary value for $\Delta F/F_0$ is only about 0.03; i.e., there is only a decrease of 3%. The time trace of $\Delta F(t)/F_0$ is the average of seven single shots. For comparison the absorption change ΔA at 360 nm is also shown in Figure 4A for the same sample. This time trace is from a single shot. ΔA is approximately zero until about 50 μs and then rises, also reaching a constant value after about 20 ms. It is apparent that the kinetics of the fluorescence decrease and absorbance increase are virtually identical up to about 50 ms. This conclusion was confirmed in a quantitative way by that fact that the two time traces could be fitted simultaneously with a sum of three exponentials with the common time constants of $\tau_1 = 410$ μs, $\tau_2 = 3.6$ ms, and $\tau_3 = 12$ ms (indicated by vertical dashed lines in Figure 4A). The fit curves are also shown in Figure 4A.

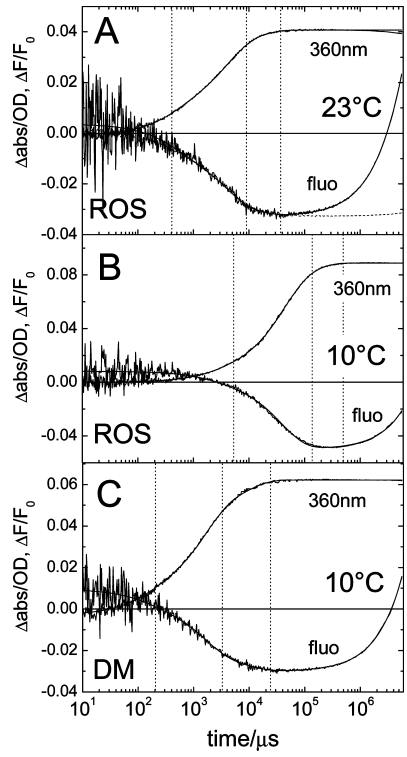

FIGURE 4: Joint presentation of the transient absorption at 360 nm and the transient Trp fluorescence of rhodopsin under different conditions: rhodopsin in washed ROS membranes in 10 mM MES buffer, pH 6, at 23 °C (A) and 10 °C (B) and in DM micelles in buffer C, pH 6, at 10 °C (C). The vertical lines indicate the time constants for a joint fit of the absorption and fluorescence data by a sum of three exponentials. To describe the fluorescence increase in the time range of seconds (due to the M_{II} decay), a fourth exponential was added in the fit of the fluorescence data. The fit curves are superimposed on the data. In panel A additionally a scaled mirror image of the transient absorption curve is shown as a dashed line to underline the similarity of the kinetics of the fluorescence and absorption signals.

Within experimental error the kinetics of the two signals are identical out to about 30 ms. Since the absorbance increase at 360 nm is due to the deprotonation of the Schiff base during the formation of M_{II}, the fluorescence decrease of the tryptophans must likewise be associated with the Schiff base deprotonation.

Beyond 100 ms and in particular after 1 s, there is a steep increase in fluorescence, which clearly continues beyond the range of the data acquisition (6 s). Measurements with a time range extending out to 200 s and at a reduced intensity of the 280 nm excitation light show that at 200 s the fluorescence increase has an amplitude that is more than ten times that of the initial negative component and is still increasing (data not shown). Under these conditions the exponential time constant of this positive component was estimated to be 350 s. This very large fluorescence increase is due to the loss of energy transfer when the retinal is released from the binding pocket after hydrolysis of the Schiff base during the decay of M_{II}. This slow increase in tryptophan fluorescence is well-known (*20, 21*) and is used as an assay to monitor the decay of $Meta_{II}$ (*20, 21*). The time constant we observed is in accordance with previous reports (*20, 21*).

Figure 4B shows the results of corresponding measurements at 10 °C. From 1 μs to about 1 ms the change is again close to zero. At this lower temperature the rise of M_{II} is slower than at 23 °C. The kinetics of the fluorescence decrease and absorbance increase are again synchronized and can be fitted simultaneously with a sum of three exponentials with common time constants of $\tau_1 = 2.3$ ms, $\tau_2 = 38$ ms, and $\tau_3 = 116$ ms. The positive phase of the fluorescence increase is also slowed down with respect to its time trace at 23 °C, in agreement with the known temperature dependence of the decay of M_{II} (*21*).

Transient Tryptophan Fluorescence in DM Micelles. Similar experiments were performed with monomeric rhodopsin in DM micelles (at pH 6). Whereas in ROS membranes energy transfer between adjacent rhodopsin molecules (e.g., dimers) may contribute to the fluorescence signal, this can be excluded in micelles. Since the formation of M_{II} is faster in DM micelles than in ROS membranes, the DM data have a lower signal-to-noise ratio. The results of Figure 4C are nevertheless qualitatively the same as for ROS membranes. The kinetics of the fluorescence and absorbance change matched again in the time range from 10 μs to 20 ms at 10 °C. The global fit resulted in $\tau_1 = 136$ μs, $\tau_2 = 1.5$ ms, and $\tau_3 = 8.4$ ms at 10 °C. Similar data (not shown) were obtained at 23 °C which are, however, noisier due to the accelerated kinetics at this temperature ($\tau_1 = 93$ μs and $\tau_2 = 2.5$ ms at 23 °C). A positive fluorescence component was again observed for times longer than seconds. This fluorescence increase reflects the decay of M_{II}.

Energy Transfer from Tryptophan to the Retinylidene Chromophore. It is well-known that the fluorescence of the five tryptophans of rhodopsin is strongly quenched in the dark state by energy transfer to the retinylidene chromophore (*19*−*21*). The average fluorescence quantum yield of the tryptophans in opsin is for example between two and four times larger than in rhodopsin (*20, 21*), suggesting that more than half the tryptophans are completely quenched in the dark state. According to eqs 1 and 2 the rate of energy transfer is proportional to the spectral overlap integral J of the donor/acceptor pair and to the κ^2 factor which describes the angular dependence of the transition dipole moment interaction. It is moreover inversely proportional to R_{DA}^6, where R_{DA} is the donor−acceptor distance. In M_I ($\lambda_{max} \approx$ 480 nm), the spectral overlap integral does not differ much from that in the dark state ($\lambda_{max} \approx 500$ nm). Moreover, the structure of M_I is not significantly different from that of rhodopsin (*6*). In particular, all the tryptophan residues and the β-ionone ring of the retinal in M_I are in the same positions as in rhodopsin, with the possible exception of W265 (*6*). This residue does not contribute, however, to the fluorescence (see below). A transient change in fluorescence in the time range up to 100 μs is thus only expected if there are significant changes in the κ^2 value between rhodopsin and M_I. As the retinal isomerizes upon photoactivation, this may occur for an individual Trp−retinal pair, but for an ensemble of tryptophans with positive and negative changes in κ^2 these effects tend to cancel out. In M_{II} ($\lambda_{max} \approx 380$ nm), however, the spectral overlap increases by a factor of about 2.4 (see also Figure 5), leading to an increase in energy transfer if the structural parameters (κ^2, R_{DA}) remain roughly the same. On the basis of this argument we expect a decrease in tryptophan fluorescence which is exactly synchronized with the formation of M_{II}. This is indeed what was observed.

Two questions remain. Which tryptophans contribute to this fluorescence change? This question cannot be answered

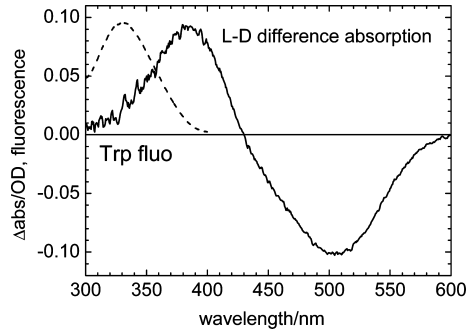

FIGURE 5: M_{II}−rhodopsin light minus dark difference absorption spectrum obtained after photoconversion of ROS membranes at pH 6 (solid line). The dashed line is the tryptophan emission spectrum of rhodopsin. This figure illustrates the increase in spectral overlap of the tryptophan emission in the rhodopsin to M_{II} transition.

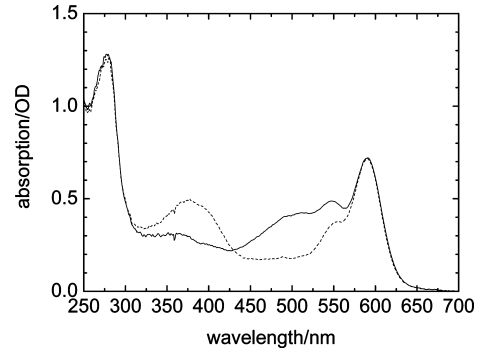

FIGURE 6: Absorption spectra of Alexa594-labeled ROS membranes before (solid line) and immediately after illumination with an LED emitting at 470 nm (dashed line). Conditions: 10 mM MES, pH 6.0, room temperature.

at this point, but we can evaluate which tryptophans contribute to the signal in the dark state. The κ^2 factors (eq 2) can be determined from the published crystal structures of rhodopsin (*2*−*4*). This requires knowledge about the way the transition dipole moments are fixed in the molecular frameworks of donors and acceptors. For the tryptophan donor and retinylidene acceptor this is well-known and discussed in refs *31* and *32*, respectively. The transient dipole moment geometry for the pair W161 and the chromophore is shown in Figure 3. We can then calculate the Förster radii R_0 for each tryptophan−retinal pair using the κ^2 values and the measured spectral overlap integral *J*. These values are listed in Table 1 together with R_{DA} and κ^2 for the crystal structure of rhodopsin with the highest available resolution of 2.2 Å (*4*). The last column of Table 1 lists the ratio of the fluorescence lifetime τ_i and the lifetime in the absence of energy transfer τ_D. This ratio was calculated from the values of R_0 and R_{DA} and expresses the degree of quenching by energy transfer. One means no energy transfer. Zero means complete energy transfer. For W265 and W126 the distance R_{DA} is much smaller than R_0 so that these residues are already completely quenched in the dark state. The very efficient energy transfer from these two residues thus provides the main explanation for the fact that the fluorescence quantum yield of opsin is at least twice as large as in rhodopsin (*20, 21*). For W35 and W175 the distances are comparable to R_0 so that these residues are partially quenched in the dark state and sensitive to changes in energy transfer in intermediate states such as M_{II}. W161 is not quenched due to the fact that κ^2 is very close to zero. A very small change in orientation of the indole side chain of this residue or of retinal will thus lead to quenching of its fluorescence. The second question concerns the small size of the observed change of 3−5%. From the increase in spectral overlap in M_{II} alone, we expect a decrease in fluorescence of about 18%, considerably more than observed, but consistent with a decrease of about 12% detected in steady-state measurements (*20*). There are several explanations for this discrepancy. The main reason is that the sample is not bleached completely by the single flash (about 60%). Another reason is that as soon as the 280 nm excitation light is turned on, before arrival of the excitation flash and the start of the data acquisition, the sample begins to bleach via the ultraefficient energy transfer from W265 and W126 to the retinylidene chromophore.

Transient Fluorescence of Helix 8 Labeled at Cysteine 316 with Alexa594. Helix 8 of rhodopsin in ROS membranes was selectively labeled at cysteine 316 with Alexa594-maleimide as described (*23*). There it was shown that when the molar ratio of Alexa594 to rhodopsin in the reaction mixture is 2.3 or below, only cysteine 316 is labeled. At the mixing ratio of 2.3 a bound label to rhodopsin ratio of 0.93 was obtained (*23*). In our experiment we used the same labeling protocol with a mixing ratio of 2. Absorption spectra of the labeled rhodopsin in the dark and after bleaching of rhodopsin are shown in Figure 6. These spectra are very similar to those shown in ref *23* for a labeling stoichiometry of 0.93. From the ratio of the maximal absorbance of the label (at 594 nm) and rhodopsin (at 500 nm) and the known extinction coefficients we estimated a dye to rhodopsin ratio of 0.95. Proof that the labeling site was cysteine 316 was obtained by thermolysin cleavage followed by fluorescence detection of the long and short fragments containing cysteine 140 and cysteine 316, respectively (*23*). It is well established that cysteine 316 is more reactive than cysteine 140 and that under appropriate conditions only cysteine 316 is labeled (*33*−*35*).

In previous work (*23*) the fluorescence increased by about 20% upon bleaching of rhodopsin (at pH 6), but this change could not be resolved in time. Since the pH dependence of the amplitude of the Alexa594 fluorescence increase roughly matched the pH dependence of the M_I/M_{II} equilibrium, it was conjectured (*23*) that it probably was kinetically correlated with the rise of M_{II}. Here we use transient fluorescence to time-resolve the increase in fluorescence. The fluorescence of the labeled ROS membranes was excited with an LED emitting at 590 nm. The transient fluorescence was observed after excitation of rhodopsin with an intense 10 ns laser flash at 460 nm. Typical data from a single shot excitation at pH 6 and 23 °C are shown in Figure 7A. The fluorescence increase is initially close to zero and starts to increase around 200 μs after flash excitation. It reaches its final value of 27%, comparable to the value of 20% reported earlier (*23*), at around 0.1−1 s. This value depends on the exact values of the labeling stoichiometry, the pH, and the temperature. To find out if the LED at 590 nm led to photoactivation of rhodopsin, we performed the following control experiment. The transient fluorescence was measured with the rhodopsin flash excitation at 460 nm blocked off. Under these conditions the time course of $\Delta F/F_0$ was zero out to a time of 1 s after the blocked flash (data not shown),

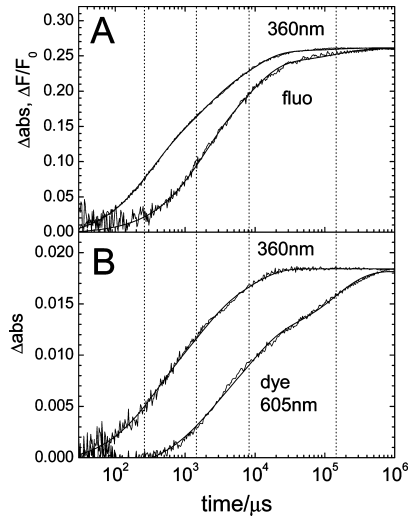

FIGURE 7: (A) Joint presentation of the transient absorption at 360 nm and the transient Alexa594 fluorescence in photoactivated ROS membranes. The time course of the transient absorption was scaled to the same end value as for the fluorescence signal. Conditions: 10 mM MES, pH 6, 23 °C. (B) Transient absorption at 360 and 605 nm of photoactivated ROS membranes in unbuffered 100 μM BCP solution. The time course of the transient 360 nm absorption was scaled to the same end value as for the 605 nm signal. Conditions: pH 6, 23 °C. The time courses of the transient fluorescence and absorbance are the averages over two or three shots. The common vertical lines indicate the time constants for a joint fit of all data sets in panels A and B by a sum of four exponentials. The fit curves are superimposed on the data; the corresponding time constants and relative amplitudes are listed in Table 2.

Table 2: Results of a Joint Fit of Transient Fluorescence (Alexa594, fluo), Transient Absorbance at 360 nm (a360), and Transient Absorbance at 605 nm (a605, Proton Uptake with Dye BCP) Data of Figure 7[a]

sample	signal	τ_1/ms	τ_2/ms	τ_3/ms	τ_4/ms	a_1	a_2	a_3	a_4
ROS-Alexa594	a360	0.26	1.4	8.2	145	0.4	0.3	0.27	0.02
	fluo					0	0.47	0.45	0.08
ROS + BCP	a360					0.35	0.40	0.25	0
	a605					0	0.25	0.42	0.33

[a] τ_1–τ_4, time constants of a joint fit of the data in Figure 7. a_1–a_4, relative amplitudes of the fit components calculated from the absolute values by normalizing them by the sum of all amplitudes of each time trace.

indicating that on this time scale no rhodopsin was photoactivated by the 590 nm LED. It is of interest to compare the transient fluorescence change with the transient absorbance change at 360 nm measured with the same sample. These results are also shown in Figure 7A. The change in absorbance is scaled in such a way that the same end value is reached as for $\Delta F/F_0$. This comparison clearly shows that in ROS membranes under these conditions the structural/environmental change in helix 8, as sensed by Alexa594, is delayed with respect to the deprotonation of the Schiff base.

At least three events occur between the decay of M_I and the decay of M_{II}: Schiff base deprotonation, a major structural change, and proton uptake from the cytoplasmic surface. It is thus of considerable interest to compare the transient fluorescence kinetics also with the kinetics of proton uptake. The latter was measured using transient absorption spectroscopy with the pH-sensitive dye bromocresol purple (BCP). The deprotonated form of BCP has its absorption maximum at 590 nm. We measured the transient absorption at 605nm because rhodopsin does not absorb at this wavelength (see the negative band in Figure 5). This choice prevents the activation of the photoreceptor by the measuring light and contributions of the protein absorbance to the transient signal. Since Alexa594 has its maximal absorbance at 594 nm, the dye experiments had to be carried out with unlabeled rhodopsin since otherwise the very high absorbance at 605 nm would preclude dye measurements of acceptable signal-to-noise ratio. The results of the transient dye measurements under the same conditions as in Figure 7A are shown in Figure 7B. The increase in absorbance at 605 nm indicates an increase in pH, corresponding to proton uptake. These measurements had to be performed in the absence of buffer. For comparison the transient absorbance change at 360 nm of the same sample (i.e., unlabeled rhodopsin) under the same conditions is also shown in Figure 7B. This time trace is virtually identical to that in the presence of the label (Figure 7A). The vertical scale in Figure 7B refers to the dye signal. The transient absorbance signal at 360 nm was scaled to reach the same end value as the dye signal. The data of Figure 7 indicate that the dye signal is further delayed with respect to the fluorescence signal. Moreover, the kinetics of all three signals are complex, containing a number of exponential components, as has been known for some time (*10, 11, 14*). The data of Figure 7 were fitted with a sum of four exponentials with common time constants. The fit curves are also shown and indicate that a satisfactory fit was achieved. The common exponential time constants are indicated by vertical dotted lines. Their values and the corresponding relative amplitudes are collected in Table 2. The amplitude values document in a quantitative way what was already clear by visual inspection of the data of Figure 7. The main cause of the delay between the Schiff base deprotonation and the structural change of helix 8 is due to the earliest component with $\tau_1 = 260$ μs. This amplitude is 40% for ΔA_{360} and 0% for $\Delta F/F_0$. For both the absorbance and fluorescence change the fourth amplitude is very small. For the unlabeled sample the amplitudes for the ΔA_{360} signal (third row) have relative amplitudes that are similar to those of the labeled sample, as expected. The fourth row contains the relative amplitudes for the dye signal (ΔA_{605}). As for the fluorescence, $A_1 = 0$. The main cause for the delay with respect to the fluorescence is the large contribution of $A_4 = 0.33$ with the longest time constant of 145 ms. This component is absent in the kinetics of the Schiff base deprotonation and of small amplitude in the fluorescence increase. Irrespective of the analysis with a sum of exponentials, the data themselves are of sufficient signal-to-noise ratio to allow the conclusion that the fluorescence signal is delayed with respect to the absorbance change at 360 nm and that the dye signal is further delayed with respect to the fluorescence signal. Due to the logarithmic time scale the differences in kinetics appear to be smaller than they are.

The temperature dependence of the kinetics of these three signals (Schiff base deprotonation, structural change of helix 8, and proton uptake) was measured between 5 and 39 °C (data not shown). At each temperature the time order of the three traces was as at 23 °C (Figure 7): the rise of M_{II} is fastest, followed by the rise of the fluorescence, followed by the dye signal. With increasing temperature the proton signal lagged further behind the fluorescence signal. Re-

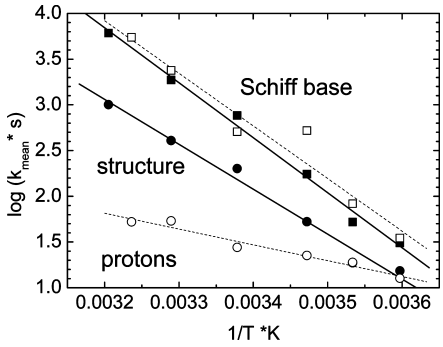

FIGURE 8: Arrhenius plots of the mean kinetics of the retinal protonation (squares), the structural change at helix 8 (filled circles), and the proton uptake from the solvent (open circles). The kinetics of the Schiff base deprotonation were derived from the transient 360 nm absorption measurements in the Alexa594 fluorescence experiment (■) and the proton uptake experiment (□). The kinetics of the structural change in helix 8 was derived from the transient Alexa594 fluorescence (●) and the kinetics of the proton uptake from the transient BCP absorption at 605 nm (○). The mean logarithmic rates were calculated as described in the text. Linear fits of the mean logarithmic rates are shown as solid lines for the Alexa594 fluorescence experiment (labeled sample) and as dashed lines for the proton uptake experiment (unlabeled sample). The corresponding activation energies are listed in the text.

cently, the temperature dependence of the kinetics of Schiff base deprotonation, of the structural change (ESR), and of the proton uptake was compared for rhodopsin in DM micelles (*9*). Due to their lower signal-to-noise ratio and a narrower time window those data could be fitted with single exponentials. Since in ROS membranes the kinetics contain multiple components with individual rate constants, a direct comparison with the DM results of ref *9* is not possible, unless we make the following simplifying assumption. The multicomponent kinetics may be approximated by a single component with the average effective rate constant $\bar{k}$ defined by

$$\log \bar{k} = \sum_i A_i \log k_i \qquad (3)$$

where A_i is the normalized amplitude of the ith component. The logarithm of this average rate constant is plotted versus 1/T in Figure 8 for each signal. The resulting Arrhenius plots are to a good approximation linear. For the Schiff base deprotonation there are two Arrhenius plots, for labeled and unlabeled rhodopsin. As expected, these are almost identical. The plots for the Schiff base deprotonation have the steepest slopes and the largest activation energy (115 and 110 kJ/mol). The activation energy for the structural change is somewhat smaller (94 kJ/mol), whereas that of the proton uptake is much smaller (33 kJ/mol). As a consequence, the Arrhenius plots for the fluorescence and the dye signals cross near 5 °C. At the highest temperature of 39 °C the effective rate constant for proton uptake is more than ten times slower than for the structural change as sensed by Alexa594. The fluorescence change in turn is about six times slower than the deprotonation of the Schiff base.

DISCUSSION

In this study we applied the method of transient fluorescence for the first time to rhodopsin. We demonstrated its utility with the natural tryptophan chromophores as well as with rhodopsin labeled at cysteine 316 in helix 8 with Alexa594. We showed that we can obtain new kinetic information about protein dynamics as sensed at these sites. In the past the kinetics of the photocascade of rhodopsin has been mainly investigated by transient electronic absorption spectroscopy, which provides information on the transitions between the various photointermediates based on differences in their chromophore absorption spectra. Transient fluorescence has the advantage that it can report on localized structural or environmental changes at any site in rhodopsin that can be specifically labeled with a suitable fluorophore (here the five tryptophans and Alexa-labeled cysteine 316). In this respect it is similar to transient ESR spectroscopy with spin labels which was recently applied to monitor the kinetics of the tilting of helix VI on the millisecond time scale (*9*). Since fluorescence is more sensitive than ESR, data of better signal-to-noise ratio and time resolution can be obtained with transient fluorescence.

Transient Fluorescence of Tryptophans. In the dark state the tryptophan fluorescence of rhodopsin is strongly quenched by energy transfer to the retinylidene acceptor (*19*−*21*). During the decay of M_{II}, the Schiff base hydrolyzes and retinal is released from the binding pocket. In the absence of the acceptor the donor fluorescence is much larger. This increase in fluorescence which occurs on the time scale of 15 min has been used as an assay to monitor the kinetics of the M_{II} decay (*20, 21*). A steady-state emission spectrum taken immediately after the bleach indicated, however, that the initial emission was less than in the dark (*20*). Here we used transient fluorescence to time-resolve this fluorescence decrease from microseconds to seconds using a logarithmic time base.

In the early microsecond time range the fluorescence change was close to zero, suggesting that prior to M_{II} formation no significant structural or environmental changes occur for those tryptophans that contribute to the signal and that there are no significant changes in the direction of the transition dipole moment of the retinal which would lead to a net change in the κ^2 values of the donor−acceptor pairs. This conclusion is in agreement with the low-resolution structure of M_I in which the bulky tryptophan residues and the β-ionone ring of the retinal were resolved (*6*).

From 100 μs onward, our results with rhodopsin in ROS membranes and DM micelles and at various temperatures show that the kinetics of the tryptophan fluorescence decrease are identical to that of the chromophore absorbance increase at 360 nm. The fluorescence decrease is apparently synchronized with the deprotonation of the Schiff base and the formation of M_{II}.

To gain some insight into the relative contributions from the five tryptophans to the energy transfer, we used the crystal structure of the dark state (*2*−*4*) to calculate the κ^2 factor for each tryptophan−retinal pair. Together with the measured spectral overlap integral this allowed us to calculate the Förster radius for each donor−acceptor pair. Comparing these values with the donor−acceptor distances from the crystal structure (Table 1), we concluded that W265 and W126, the tryptophans closest to the retinal, are already completely quenched in the dark state. The remaining three, W35, W161, and W175, are partially quenched by energy transfer and thus still sensitive to changes in structure or overlap. In M_{II} the spectral overlap integral J increases

significantly (factor 2.4) since the absorption maximum is blue shifted to 380 nm (Figure 5). Thus we expect a decrease in fluorescence that is synchronized with the rise of M_{II} just from the increase in J alone (i.e., without any structural changes reflected in κ^2 and/or R_{DA}). The rise of M_{II} is a direct measure of the increase in J. κ^2 and R_{DA} may of course also change in M_{II}. The deprotonation of the Schiff base and the proton transfer to E113 are localized events, however, that probably do not lead to changes in κ^2 and R_{DA} of the tryptophans except for W265 (*26*). The subsequent structural change, however, which involves a tilt of helix VI may well lead to changes in these two factors. Such a contribution is expected to be delayed, however, with respect to the Schiff base deprotonation (*9*), contrary to observation. A prime candidate to sense the structural change of helix VI is W265, one of the residues of this helix. As explained above, however, this tryptophan is already completely quenched in the dark and will not contribute to the fluorescence signal in M_{II}. The same holds for W126 in helix III. The remaining three tryptophans are further away from the binding pocket and in helices I and IV which do not experience major structural changes (*12*). It is thus likely that the fluorescence decrease is almost entirely due to the change in J.

This analysis is consistent with light minus dark difference spectra in the tryptophan UV absorption bands (*27*). Using single tryptophan mutants, these authors showed that the observed difference spectrum is due to environmental perturbations of W265 and W126 in the formation of M_{II}. The other three tryptophans, which are the ones we observe in our fluorescence experiment, did not contribute to the UV absorbance difference spectra (*27*), suggesting that they do not undergo structural/environmental changes.

Strong evidence for movement and rotation of the indole ring of W265 in the formation of M_{II} was obtained from solid-state NMR (*26*). Earlier linear dichroism studies had already shown that the indole side chain of the tryptophan closest to the retinylidene chromophore rotates by about 90° in the formation of M_{II} (*25*). Due to strong energy transfer this motion of W265 is not observable via its fluorescence.

The fluorescence decrease associated with the rise of M_{II} is followed by a much slower increase of larger amplitude that continues well beyond our measuring range with an estimated exponential rise time of 350 s. This component is clearly due to the decay of M_{II} in which hydrolysis of the Schiff base and release of retinal from the binding pocket lead to a complete loss of the energy transfer.

Transient Fluorescence of Alexa594 in Helix 8. Helix 8 is an amphipathic helix that runs parallel to the cytoplasmic surface from Asn 310 to Cys 322 (*2*−*4*). It plays an essential role in the interaction of rhodopsin with transducin (*36*) and is considered to be a surface recognition domain (*37*). Evidence for light-induced structural changes of helix 8 comes from spin label (*38, 39*), time-resolved fluorescence depolarization (*33*), steady-state fluorescence (*23*), FTIR (*40*), and mutagenesis (*41*) experiments. From studies with model peptides it was suggested that H8 may lose its helical structure upon illumination and adapt a looplike structure upon activation, thus acting as a conformational switch (*37*).

Since its excitation maximum is well to the red of that of rhodopsin, the fluorescent dye Alexa594 allows steady-state fluorescence measurements without significant bleaching of rhodopsin (*23*). It was reported that cysteine 316 in helix 8 could be specifically labeled with Alexa594 in ROS membranes and that the function of rhodopsin (interaction with transducin and arrestin) is not impaired (*23*). In particular, it was shown that the M_I/M_{II} equilibrium had the normal pK_a, that the extra-M_{II} effect was present, and that the binding affinity for transducin was not affected by the labeling (*23*). In the M_I/M_{II} equilibrium the fluorescence was 20% higher than in the dark state under conditions that maximize M_{II} (*23*). Since the fluorescence was only 3% higher when the pH was increased to values where the equilibrium is dominated by M_I, it was hypothesized that the increased fluorescence is due to M_{II}. Here we time-resolved the rise of the fluorescence and investigated whether this structural/environmental change at cysteine 316 is kinetically coupled to the Schiff base deprotonation as suggested in ref *23* or to the transient proton uptake.

Our results (Figure 7A, Table 2) indicate that in ROS membranes (pH 6, 23 °C) the kinetics of the structural/environmental change as sensed at cysteine 316 is significantly delayed with respect to the Schiff base deprotonation. The difference in kinetics is mainly due to the absence of a contribution in the fluorescence signal from the earliest 260 μs component, which contributes 40% to the rise of M_{II}. Comparison with the dye signal shows (Figure 7B, Table 2) that proton uptake from solution lags further behind the structural change. This difference is mainly due to the large contribution (33%) of the slowest component (145 ms) which is absent in the transient absorbance and quite small in the transient fluorescence. Our data thus support the following temporal sequence of events: Schiff base deprotonation, structural/environmental change at the cytoplasmic surface in helix 8, and proton uptake from solution. Our results are in accordance with the following sequential scheme that was

$$\underset{500\ nm}{Rho} \rightsquigarrow \underset{480\ nm}{M_I} \overset{\text{SB deprotonation}}{\rightleftharpoons} \underset{380\ nm}{M_{II_a}} \overset{\text{Stuctural change}}{\rightleftharpoons} \underset{380\ nm}{M_{II_b}} \overset{\text{Proton uptake}}{\rightleftharpoons} \underset{380\ nm}{M_{II_b} - H^+}$$

recently proposed for rhodopsin in DM micelles (*9*). Due to the back-reactions this scheme implies multiple exponential components in the kinetics which we actually observed in all three of our signals but which were absent in the data of ref *9*. In the study with DM micelles (*9*), the structural change was measured by ESR spectroscopy with a spin label at R227 (helix V) whereas the Schiff base deprotonation and proton uptake were monitored in the same way as here. The results with ROS membranes and DM micelles (at pH 6, 23 °C) are in agreement concerning the delay between Schiff base deprotonation and structural change. There is, however, a significant difference between the two systems concerning the proton uptake kinetics. With DM micelles the time courses of the structural change and proton uptake were the same, whereas with ROS membranes the proton uptake lagged significantly behind and was more clearly a consequence of the structural change. The temperature dependencies of structural change and proton uptake also differ markedly in the two systems. We obtained activation energies of 94 and 33 kJ/mol, respectively, for the structural change and proton uptake in ROS membranes. In DM micelles these activation energies are the same (*9*). We monitored the structural change at cysteine 316 on the cytoplasmic surface, the same surface from which the proton is presumably taken up.

There are some experimental aspects that may explain the differences between the results for ROS membranes and DM micelles. The ROS results extended over a much larger time range (5 decades of time, using logarithmic time base) and had a higher S/N ratio. The ROS data were clearly multiexponential, containing three or four components, whereas the noisier DM data were fitted with a single exponential over a much narrower time range (0−5 or 0−20 ms for the optical and ESR signals, respectively). The multiexponential character of our data prevented the construction of a single Arrhenius plot. For the purpose of comparison with the DM Arrhenius plots, we therefore formed the logarithmic average of the three rate constants and used this in an average Arrhenius plot. The resulting plots are linear (Figure 8) and resemble the corresponding DM plots (*9*) in many respects. The activation energies for the Schiff base deprotonation are similar, as well as the crossover near 5 °C. In fact, the activation energies which we estimated from Figure 4 of ref *9* for the SB deprotonation, 120 and 127 kJ/mol, are remarkably close to those of our Figure 8 (110 and 115 kJ/mol), suggesting that our logarithmic averaging procedure is not unreasonable. We find, however, that at physiological temperatures proton uptake lags significantly behind the structural change in helix 8 in ROS membranes, whereas these reactions have the same kinetics in DM micelles (*9*). This discrepancy may of course also be due to differences in the rhodopsin samples. In the native ROS membranes rhodopsin resides in a lipid bilayer and is surrounded by neighboring rhodopsin molecules. The delayed proton uptake at the cytoplasmic surface of ROS membranes may be due to lipid surface charge effects which are absent in the micelles.

REFERENCES

1. Palczewski, K. (2006) G Protein-coupled receptor rhodopsin. *Annu. Rev. Biochem. 75*, 743–767.
2. Palczewski, K., Kumasaka, T., Hori, T., Behnke, C. A., Motoshima, H., Fox, B. A., Le Trong, I., Teller, D. C., Okada, T., Stenkamp, R. E., Yamamoto, M., and Miyano, M. (2000) Crystal structure of rhodopsin: a G protein-coupled receptor. *Science 289*, 739–745.
3. Li, J., Edwards, P. C., Burghammer, M., Villa, C., and Schertler, G. F. X. (2004) Structure of bovine rhodopsin in a trigonal crystal form. *J. Mol. Biol. 343*, 1409–1438.
4. Okada, T., Sugihara, M., Bondar, A. N., Elster, M., Entel, P., and Buss, V. (2004) The retinal conformation and its environment in rhodopsin in light of a new 2.2 Å crystal structure. *J. Mol. Biol. 342*, 571–583.
5. Murakami, M., and Kouyama, T. (2008) Crystal structure of squid rhodopsin. *Nature 453*, 363–367.
6. Ruprecht, J. J., Mielke, T., Vogel, R., Villa, C., and Schertler, G. F. X. (2004) Electron crystallography reveals the structure of metarhodopsin I. *EMBO J. 23*, 3609–3620.
7. Nakamichi, H., and Okada, T. (2006) Local peptide movement in the photoreaction intermediate of rhodopsin. *Proc. Natl. Acad. Sci. U.S.A. 103*, 12729–12734.
8. Kukura, P., McCamant, D. W., Yoon, S., Wandschneider, D. B., and Mathies, R. A. (2005) Structural observation of the primary isomerization in vision with femtosecond-stimulated Raman. *Science 310*, 1006–1009.
9. Knierim, B., Hofmann, K. P., Ernst, O. P., and Hubbell, W. L. (2007) Sequence of late molecular events in the activation of rhodopsin. *Proc. Natl. Acad. Sci. U.S.A. 104*, 20290–20295.
10. Dickopf, S., Mielke, T., and Heyn, M. P. (1998) Kinetics of light-induced proton translocation associated with the pH-dependent formation of the metarhodopsin I/II equilibrium of bovine rhodopsin. *Biochemistry 37*, 16888–16897.
11. Thorgeirrson, T. E., Lewis, J. W., Wallace-Williams, S. E., and Kliger, D. S. (1993) Effects of temperature on rhodopsin photointermediates from lumirhodopsin to metarhodopsin II. *Biochemistry 32*, 13861–13872.
12. Altenbach, C., Kusnetzow, A. K., Ernst, O. P., Hofmann, K. P., and Hubbell, W. L. (2008) High-resolution distance mapping in rhodopsin reveals the pattern of helix movement due to activation. *Proc. Natl. Acad. Sci. U.S.A. 105*, 7439–7444.
13. Arnis, S., and Hofmann, K. P. (1993) Two different forms of metarhodopsin II: Schiff base deprotonation precedes proton uptake and signaling state. *Proc. Natl. Acad. Sci. U.S.A. 90*, 7849–7853.
14. Szundi, I., Mah, T. L., Lewis, J. W., Jäger, S., Ernst, O. P., Hofmann, K. P., and Kliger, D. S. (1998) Proton transfer reactions linked to rhodopsin activation. *Biochemistry 37*, 14237–14244.
15. Armis, D., Fahmy, K., Hofmann, K. P., and Sakmar, T. P. (1994) A conserved carboxylic acid group mediates light-dependent proton uptake and signaling by rhodopsin. *J. Biol. Chem. 269*, 23879–23881.
16. Vogel, R., Mahalingam, M., Lüdeke, S., Huber, T., Siebert, F., and Sakmar, T. P. (2008) Functional role of the "ionic lock"—an interhelical hydrogen bond network in family A heptahelical receptors. *J. Mol. Biol. 380*, 648–655.
17. Farahbakhsh, Z. T., Hideg, K., and Hubbell, W. L. (1993) Photoactivated conformational changes in rhodopsin: a time-resolved spin label study. *Science 262*, 1416–1419.
18. Lüdeke, S., Lórenz Fonfria, V A., Siebert, F., and Vogel, R. (2006) Time-resolved rapid-scan Fourier transform infrared difference spectroscopy on a noncyclic photosystem: rhodopsin photointermediates from Lumi to Meta II. *Biopolymers 83*, 159–169.
19. Ebrey, T. G. (1971) Energy transfer in rhodopsin, N-retinyl-opsin and rod outer segments. *Proc. Natl. Acad. Sci. U.S.A. 68*, 713–716.
20. Farrens, D. L., and Khorana, H. G. (1995) Structure and function of rhodopsin.Measurement of the rate of metarhodopsin II decay by fluorescence spectroscopy. *J. Biol. Chem. 270*, 5073–5076.
21. Heck, M., Schädel, S. A., Maretzki, D., Bartl, F. J., Ritter, E., Palczewski, K., and Hofmann, K. P. (2003) Signaling states of rhodopsin. *J. Biol. Chem. 278*, 3162–3169.
22. Bartl, F. J., and Vogel, R. (2007) Structural and functional properties of metarhodopsin III: recent spectroscopic studies on deactivation pathways of rhodopsin. *Phys. Chem. Chem. Phys. 9*, 1648–1658.
23. Imamoto, Y., Kataoka, M., Tokunaga, F., and Palczewski, K. (2000) Light-induced conformational changes of rhodopsin probed by fluorescent alexa594 immobilized on the cytoplasmic surface. *Biochemistry 39*, 15225–15233.
24. Hoersch, D., Otto, H., Cusanovich, M. A., and Heyn, M. P. (2008) Distinguishing chromophore structures of photocycle intermediates of the photoreceptor PYP by transient fluorescence and energy transfer. *J. Phys. Chem. B 112*, 9118–9125.
25. Chabre, M., and Breton, J. (1979) Orientation of aromatic residues in rhodopsin.Rotation of one tryptophan upon meta I to meta II transition after illumination. *Photochem. Photobiol. 30*, 295–299.
26. Crocker, E., Eilers, M., Ahuja, S., Hornak, V., Hirshfeld, A., Sheves, M., and Smith, S. O. (2006) Location of trp265 in metarhodopsin II: implications for the activation mechanism of the visual receptor rhodopsin. *J. Mol. Biol. 357*, 163–172.
27. Lin, S. W., and Sakmar, T. P. (1996) Specific tryptophan UV-absorbance changes are probes of the transition of rhodopsin to its active state. *Biochemistry 35*, 11149–11159.
28. McDowell, J. H., and Kühn, H. (1977) Light-induced phosphorylation of rhodopsin in cattle photoreceptor membranes: substrate activation and inactivation. *Biochemistry 16*, 4054–4060.
29. Sommer, M. E., Smith, W. C., and Farrens, D. L. (2006) Dynamics of arrestin-rhodopsin interactions: acidic phospholipids enable binding of arrestin to purified rhodopsin in detergent. *J. Biol. Chem. 281*, 9407–9417.
30. Borucki, B., Otto, H., and Heyn, M. P. (1999) Reorientation of the retinylidene chromophore in the K, L and M intermediates of bacteriorhodopsin from time-resolved linear dichroism: Resolving kinetically and spectrally overlapping intermediates of chromoproteins. *J. Phys. Chem. B 103*, 6371–6383.
31. Otto, H., Hoersch, D., Meyer, T. E., Cusanovich, M. A., and Heyn, M. P. (2005) Time-resolved single tryptophan fluorescence in photoactive yellow protein monitors changes in chromophore structure during the photocycle via energy transfer. *Biochemistry 44*, 16804–16816.
32. Heyn, M. P., Borucki, B., and Otto, H. (2000) Chromophore reorientation during the photocycle of bacteriorhodopsin: experimental methods and functional significance. *Biochim. Biophys. Acta 1460*, 60–74.

33. Mielke, T., Alexiev, U., Gläsel, M., Otto, H., and Heyn, M. P. (2002) Light-induced changes in the structure and accessibility of the cytoplasmic loops of rhodopsin in the activated M_{II} state. *Biochemistry 41*, 7875–7884.
34. Albert, A. D., Watts, A., Spooner, P., Groebner, G., Young, J., and Yeagle, P. L. (1997) A distance measurement between specific sites on the cytoplasmic surface of bovine rhodopsin in rod outer segment disk membranes. *Biochim. Biophys. Acta 1328*, 74–82.
35. Mielke, T., Villa, C., Edwards, P. C., Schertler, G. F. X., and Heyn, M. P. (2002) X-ray diffraction of heavy-atom labeled two-dimensional crystals of rhodopsin identifies the position of cysteine 140 in helix 3 and cysteine 316 in helix 8. *J. Mol. Biol. 316*, 693–709.
36. Marin, E. P., Krishna, A. G., Zvyaga, T. A., Isele, J., Siebert, F., and Sakmar, T. P. (2000) The amino terminus of the fourth cytoplasmic loop of rhodopsin modulates rhodopsin-transducin interaction. *J. Biol. Chem. 275*, 1930–1936.
37. Krishna, A. G., Menon, S. T., Terry, T. J., and Sakmar, T. P. (2002) Evidence that helix 8 of rhodopsin acts as a membrane-dependent conformational switch. *Biochemistry 41*, 8298–8309.
38. Altenbach, C., Klein-Seetharaman, J., Cai, K., Khorana, H. G., and Hubbell, W. L. (2001) Structure and function in rhodopsin: mapping light-dependent changes in distance between residue 316 in helix 8 and residues in the sequence 60−75, covering the cytoplasmic ends of helices TM1 and TM2 and their connection loop CL1. *Biochemistry 40*, 15493–15500.
39. Altenbach, C., Cai, K., Klein.Seetharaman, J., Khorana, H. G., and Hubbell, W. L. (2001) Structure and function in rhodopsin: mapping light-dependent changes in distance between residue 65 in helix TM1 and residues in the sequence 306−319 at the cytoplasmic end of helix TM7 and in helix H8. *Biochemistry 40*, 15483–15492.
40. Lehman, N., Alexiev, U., and Fahmy, K. (2007) Linkage between the intramembrane H-bond network around aspartic acid 83 and the cytosolic environment of helix 8 in photoactivated rhodopsin. *J. Mol. Biol. 366*, 1129–1141.
41. Fritze, O., Filipek, S., Kuksa, V., Palczewski, K., Hofmann, K. P., and Ernst, O. P. (2003) Role of the conserved NPxxY(x) $_{5,6}$F motif in the rhodopsin ground state and during activation. *Proc. Natl. Acad. Sci. U.S.A. 100*, 2290–2295.
42. Borucki, B., Devanathan, S., Otto, H., Cusanovich, M. A., Tollin, G., and Heyn, M. P. (2002) Kinetics of proton uptake and dye binding by photoactive yellow protein in wild type and in the E46Q and E46A mutants. *Biochemistry 41*, 10026–10037.

BI801397E